Nanocoral-like composite of nickel selenide nanoparticles anchored on two-dimensional multi-layered graphitic carbon nitride: A highly efficient electrocatalyst for oxygen evolution reaction

Shuai Wang[a], Ping He[a,b,*], Lingpu Jia[a,*], Mingqian He[c], Tinghong Zhang[a,*], Faqin Dong[d], Mingzhang Liu[c], Huanhuan Liu[a], Ying Zhang[a], Caixia Li[a], Jun Gao[a], Liang Bian[d]

[a] State Key Laboratory for Environment-Friendly Energy Materials, School of Materials Science and Engineering, Southwest University of Science and Technology, Mianyang, 621010, PR China
[b] Mianyang Kingtiger New Energy Technology Co., Ltd., Mianyang, 621000, PR China
[c] Sichuan Changhong Battery Co., Ltd., Mianyang, 621000, PR China
[d] Key Laboratory of Solid Waste Treatment and Resource Recycle of Ministry of Education, Southwest University of Science and Technology, Mianyang, 621010, PR China

ABSTRACT

Oxygen evolution reaction is a significant half-reaction for water splitting, while its sluggish kinetics and high-cost catalyst hinder the commercial application. In this work, we report a novel nanocoral-like $NiSe_2/g-C_3N_4$ composite as highly efficient catalyst for water oxidation in 1.0 M KOH solution. Based on the support of multi-layered $g-C_3N_4$, $NiSe_2/g-C_3N_4$ composite exhibits favorable electrocatalytic performances with low overpotential of 290 mV at current density of 40 mA cm^{-2} and low onset potential of 1.38 V (vs. RHE). In addition, $NiSe_2/g-C_3N_4$ composite delivers higher current density (199 mA cm^{-2}) than those of pure $NiSe_2$ (142 mA cm^{-2}) and multi-layered $g-C_3N_4$ (112 mA cm^{-2}) at potential of 2.0 V (vs. RHE). Furthermore, $NiSe_2/g-C_3N_4$ composite exhibits an excellent long-term electrochemical stability for 10 h. The outstanding electrocatalytic properties above suggest that $NiSe_2/g-C_3N_4$ composite is a candidate for the substitution of noble metal based catalyst for oxygen evolution reaction.

1. Introduction

With the rapid growth of population and over exploitation of fossil fuels, the development of sustainable and environment-friendly energy is extremely urgent [1,2]. As one kind of energy conversion technologies, water splitting is considered as one of the holy grails of chemistry due to the facile preparation of hydrogen energy at low cost [3,4]. Water splitting contains two half-reactions: hydrogen evolution reaction at cathode and oxygen evolution reaction (OER) at anode [5,6]. Nevertheless, OER has been considered as the bottleneck for overall water splitting due to sluggish kinetics and complex four-electron oxidation process, which usually requires a large onset potential, far away from the ideal condition (1.23 V), to achieve the formation of O=O bond, thus decreasing the efficiency of hydrogen generation [7,8]. Therefore, the development of OER catalysts is imminent [9]. Admittedly, noble metal oxides based catalysts, such as IrO_2 and RuO_2, have been extensively investigated and manifested with the state-of-

the-art OER performance [10,11]. However, high cost and poor stability have constrained the widespread use of noble metal based catalysts [12,13]. To address these problems, more efforts have been devoted to develop earth-abundant elements based economical catalysts with low onset potential, low overpotential, high current density and impressive durability [14,15].

Recently, transition metal compounds, including transition metal oxide, alloys, layered hydroxide and chalcogenides, etc., are considered as promising alternative to noble metal catalysts for OER [16–20]. Among these, transition metal chalcogenides have been studied due to much covalency, small bandgaps and good band alignment with water redox levels for efficient charge transfer, thus promoting favorable catalytic efficiency [21–23]. As a member of transition metal chalcogenides, $NiSe_2$ as electrode material has attracted much attention for OER due to inherently high conductivity with a resistivity of less than 10^{-3} Ω cm, which is quite favorable for electrocatalytic water splitting [24]. Dong and co-authors have prepared a pyramid structured $NiSe_2/$

NF(Ox) with onset potential of 1.54 V (vs. RHE) [25]. Luo and co-authors have reported the $Ni_{0.5}Fe_{0.5}Se_2$ catalyst with an overpotential of 235 mV at a current density of 10 mA cm^{-2} [26]. The explorations above suggest prominent merits of $NiSe_2$ based catalyst for OER.

As well known, a suitable substrate can be selected to improve the catalytic performance of catalysts [27,28]. As one kind of support (platform or matrix) materials, $g-C_3N_4$ has been used in the field of photocatalytic water splitting due to strong visible-light absorption and suitable electronic band structure (2.7 eV) [29]. Moreover, much attention has been paid to electrocatalytic OER because of facile preparation, special layer structure and excellent chemical stability of $g-C_3N_4$ [30,31]. Qiao and co-authors have developed 3d transition metal centered $M-C_3N_4$ (M = Cr, Mn, Fe, Co, Ni, Cu, Zn) composites, which show onset potential of 1.5 V and overpotential of 380 mV to deliver the current density of 10 mA cm^{-2} in 1.0 M KOH solution [32]. It is worthwhile to develop transition metal selenides coordinated $g-C_3N_4$ composite catalysts, and thus relieving the pressure on noble mental based catalysts.

In this work, we have constructed a novel multi-layered $g-C_3N_4$ supported $NiSe_2$ ($NiSe_2/g-C_3N_4$) composite for OER through facile hydrothermal method. Pure $NiSe_2$ shows satisfied onset potential and current density, indicating intrinsically catalytic activity of $NiSe_2$. It is observed that, based on the multi-layered $g-C_3N_4$, as-prepared $NiSe_2/g-C_3N_4$ composite exhibits lower overpotential of 290 mV at the current density of 40 mA cm^{-2}, which is far less than that of $NiSe_2$ (400 mV) and $g-C_3N_4$ (540 mV), respectively. The low overpotential of $NiSe_2/g-C_3N_4$ composite suggests synergistic effect between $NiSe_2$ and multi-layered $g-C_3N_4$. This favorable composite is a promising alternative for noble-metal-free based OER catalyst.

2. Experimental

2.1. Reagents and materials

$NiCl_2·6H_2O$, $NaBH_4$, KOH, HCl, selenium power (Se, 99.9%), melamine, ethanol and acetone are analytical grade and purchased from Chengdu Chemical Reagent Factory (Chengdu, China). Polytetrafluoroethylene (PTFE, 10%) is purchased from Tianjin Chenhua Chemical Reagent Factory (Tianjin, China). Deionized water is used throughout the whole experiments.

Ni foam is purchased from Jinan Henghua Chemical Reagent Factory (Jinan, China). Ni foam substrates are treated under ultrasonication by sequentially immersing in acetone, doubly distilled water and ethanol each for 20 min, respectively, and dried at 60 °C before use.

2.2. Preparation and characterization of NiSe2/g-C3N4 based materials

2.2.1. Preparation of multi-layered g-C3N4

Multi-layered $g-C_3N_4$ was prepared by calcination process in advance. In a typical synthesis, 5.0 g melamine was placed in a semiclosed alumina crucible and heated to 550 °C in a muffle furnace for 2 h. After calcination, the collected faint yellow product (bulk $g-C_3N_4$) was stripped into multi-layered $g-C_3N_4$ by immersing in 40 mL 10% KOH solution at 60 °C for 12 h, and subsequently washed with 1.0 M HCl solution and deionized water until neutral, and finally dried at 60 °C for one night.

2.2.2. Preparation of NiSe2/g-C3N4 nanocoral composite

As shown in Scheme 1, $NiSe_2/g-C_3N_4$ composite was prepared by facile hydrothermal process. 15.0 mg as-prepared multi-layered $g-C_3N_4$ was dispersed in 20 mL deionized water with ultrasonic treatment for 30 min, followed by the addition of 4.0 mmol $NiCl_2·6H_2O$ under continuous ultrasonication for another 30 min. At the same time, 8.0 mmol Se power and 10.0 mmol $NaBH_4$ were dispersed in 50 mL deionized water with vigorous magnetic stirring for 1 h at room temperature and the solution turned to dark brown. Subsequently, Se-containing solution

and $g-C_3N_4$-containing suspension were mixed and stirred for 1 h. After that, the mixture was transferred into Teflon-lined autoclave for hydrothermal treatment at 160 °C for 12 h. The resulting product was collected by filtration, washed with deionized water and ethanol for several times and then dried at 60 °C overnight. The finally obtained composite was denoted as $NiSe_2/g-C_3N_4$. For comparison, bare $NiSe_2$ catalyst was prepared in a similar procedure without the addition of multi-layered $g-C_3N_4$.

2.2.3. Characterization of as-prepared materials

The structure of as-prepared materials was characterized by X-ray powder diffractometer (XRD, PANalytical, Netherlands) with Cu K_α radiation (λ = 0.154060 nm) and recorded from 10° to 80° at a speed of 2° min^{-1}. The morphology and composition of as-prepared materials were obtained using a scanning electron microscope (SEM, Carl Zeiss AG, Germany) equipped with an energy dispersive X-ray (EDX) analytical system. Fourier transform infrared spectra (FTIR) of fabricated materials were recorded from Nicolet 5700 (Nicolet Instrument Co., USA) in the wavenumber range of 4000–500 cm^{-1} with KBr pellet. Raman spectrum of as-prepared $g-C_3N_4$ is obtained by laser Raman spectrometer (Renishaw Instrument Co., UK) in the wavenumber range of 2000–400 cm^{-1}.

2.3. Electrode fabrication and electrochemical measurements

2.3.1. Electrode fabrication of as-prepared materials

20.0 mg as-prepared $NiSe_2/g-C_3N_4$ based material was dispersed in 1.0 mL of deionized water/ethanol/10% PTFE (1:1:1) by ultrasonic treatment for 10 min to form a uniform suspension, and then dropped onto Ni foam with an exposed area of 1.0 cm × 1.0 cm, followed by drying under vacuum at 60 °C overnight and pressing treatment with a pressure of 5.0 MPa. The final mass loading of $NiSe_2/g-C_3N_4$ composite material is calculated as 4.0 mg cm^{-2} by weighing loaded Ni foam and bared Ni foam.

#### 2.3.2. Electrochemical measurements of as-prepared materials

Electrochemical tests of polarization curves, electrochemical impedance spectroscopy (EIS) and chronoamperometry were conducted with PARSTAT 2273 electrochemical workstation (Princeton Applied Research, USA) by introducing a three-electrode system using platinum electrode as counter electrode, as-prepared electrocatalysts modified Ni foam (1.0 cm × 1.0 cm) as working electrode referred to Hg/HgO in 1.0 M KOH solution. Tafel plots were derived from polarization curves. The potential values were calibrated against the reversible hydrogen electrode (RHE) according to the Nernst equation: E_{RHE} = ($E_{Hg/HgO}$ + 0.098 V) + 0.059 pH.

3. Results and discussion

3.1. Structure, morphology and composition of as-prepared materials

3.1.1. XRD analysis

XRD analysis is performed to investigate the crystal phase of as-prepared materials. As shown in Fig. 1, the diffraction peaks at 13.22° and 27.58° correspond to (100) and (002) crystal planes of $g-C_3N_4$, respectively [33]. As for $NiSe_2$, the peaks at 30.02°, 33.68°, 36.98°, 50.84°, 55.62° and 57.90° are ascribed to main crystal planes of (200), (210), (211), (311), (023) and (321), respectively, which are well consistent with standard crystal of $NiSe_2$ (PDF # 00-041-1495) [34]. As for $NiSe_2/g-C_3N_4$ composite materials, the diffraction peaks are similar to those of bare $NiSe_2$, indicating that the crystal structure of $NiSe_2$ remains unchanged with the addition of $g-C_3N_4$. It should be noted that the small amount of $g-C_3N_4$ in composite may not satisfy the checkout of characterization [25]. The presence of $g-C_3N_4$ in $NiSe_2/g-C_3N_4$ materials can be further confirmed by the following characterization of SEM and EDX.
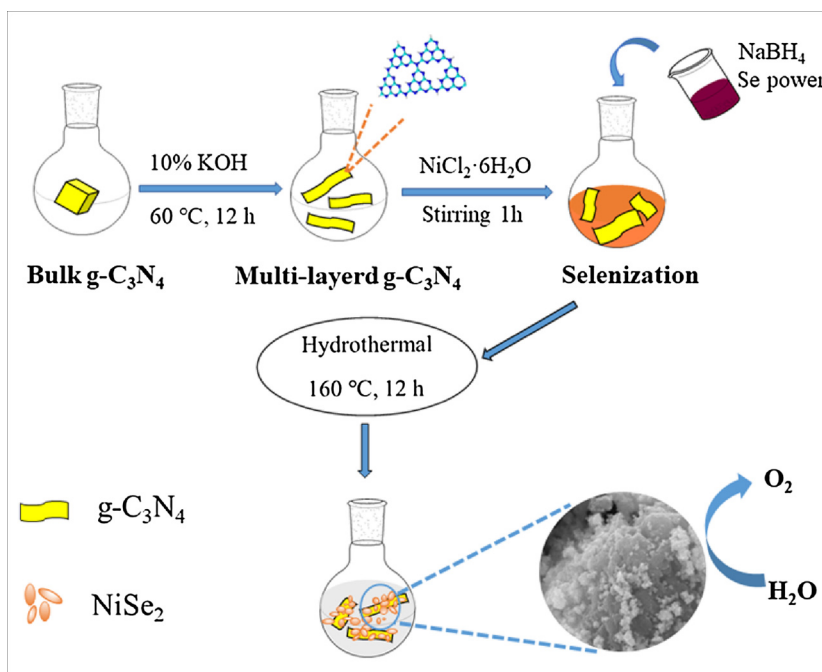
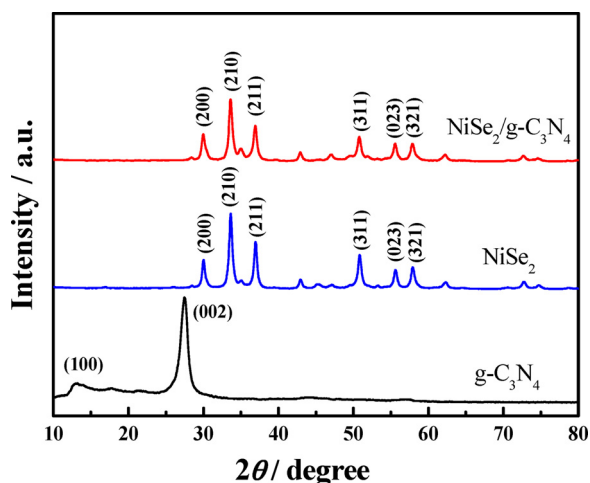**Scheme 1.** Synthesis procedure of NiSe$_2$/g-C$_3$N$_4$ composite catalyst.

Fig. 1. XRD patterns of as-prepared g-C$_3$N$_4$, NiSe$_2$ and NiSe$_2$/g-C$_3$N$_4$ materials.

3.1.2. FTIR and Raman analysis

FTIR is carried out to investigate the chemical groups of as-prepared g-C$_3$N$_4$, NiSe$_2$ and NiSe$_2$/g-C$_3$N$_4$ composite materials in the region of 4000–500 cm^{-1} (Fig. 2a). As for g-C$_3$N$_4$, the characteristic peak at 808 cm^{-1} belongs to the s-triazine ring mode and absorption peaks at 1243, 1320, 1410, 1460, 1573 and 1639 cm^{-1} are attributed to the skeletal stretching vibrations of CN heterocycles [35]. Typically, the broad band within the range of 3500–3100 cm^{-1} is related to N−H stretching vibration. Bare NiSe$_2$ and NiSe$_2$/g-C$_3$N$_4$ composite exhibit almost the same adsorption peaks, indicating that there is no structural change of NiSe$_2$ in the preparation process.

Shown in Fig. 2b is the Raman spectrum of as-prepared g-C$_3$N$_4$. The peaks at 489.2, 705.1, 760.6 and 984.5 cm^{-1} are derived from the vibration of CN, including bending mode of graphitic domains and breathing mode of s-triazine ring [36]. In addition, the peaks approximately at 1237.9 and 1564.1 cm^{-1} can be assigned to the vibration of −C−N and ring C=N, respectively [37].
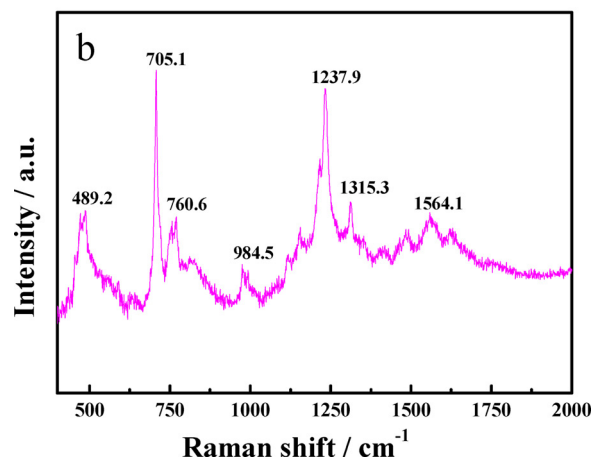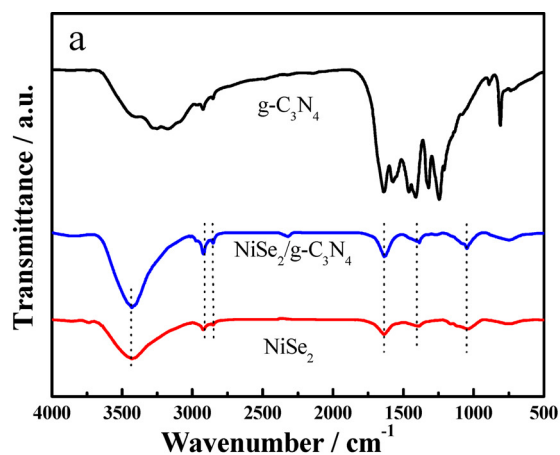

Fig. 2. FTIR spectra (a) of as-prepared g-C$_3$N$_4$, NiSe$_2$ and NiSe$_2$/g-C$_3$N$_4$ materials and Raman spectrum (b) of g-C$_3$N$_4$.
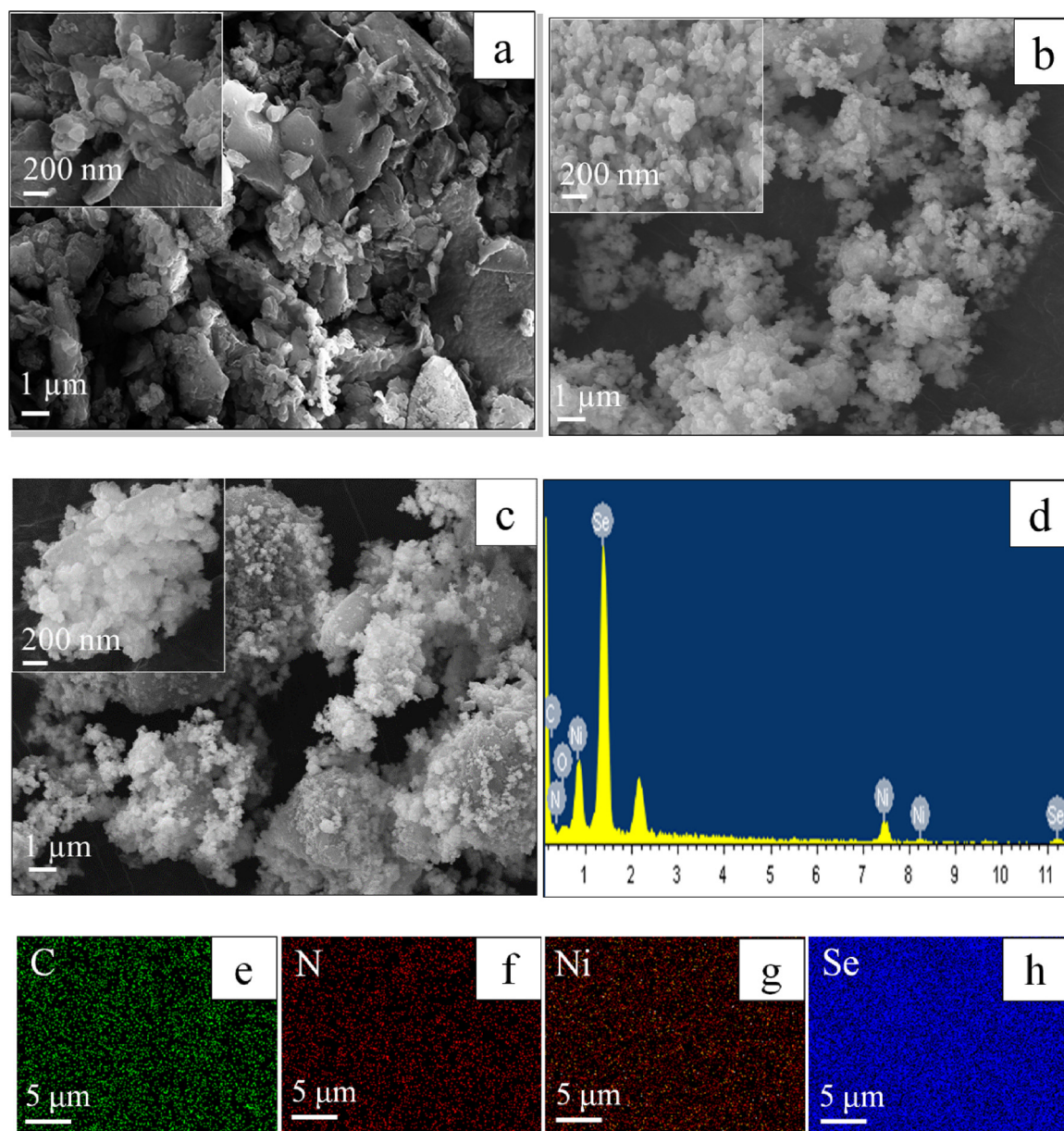
Fig. 3. SEM images of as-prepared multi-layered g-C$_3$N$_4$ (a), NiSe$_2$ nanoparticles (b) and NiSe$_2$/g-C$_3$N$_4$ nanocoral composite (c); EDX spectrum of NiSe$_2$/g-C$_3$N$_4$ nanocoral composite (d); EDX elemental mapping images of NiSe$_2$/g-C$_3$N$_4$ nanocoral composite: C (e), N (f), Ni (g) and Se (h).

3.1.3. SEM and EDX analysis

The morphologies of as-prepared materials are presented in Fig. 3. As-prepared g-C$_3$N$_4$ exhibits multi-layered morphology with rugate and rough surface, theoretically increasing the specific surface area (Fig. 3a). In addition, the multi-layered g-C$_3$N$_4$ shows a thickness of 10 ~ 20 nm (inset of Fig. 3a). As displayed in Fig. 3b, NiSe$_2$ exhibits uniformly sized nanoparticles. As shown in Fig. 3c, NiSe$_2$ nanoparticles anchor on multi-layered g-C$_3$N$_4$, resulting in nanocoral-like morphology of NiSe$_2$/g-C$_3$N$_4$ composite. Clearly, the structure of NiSe$_2$ remains unchanged with the addition of g-C$_3$N$_4$ during the hydrothermal process. Shown in Fig. 3d is the EDX spectrum of NiSe$_2$/g-C$_3$N$_4$ nanocoral composite. EDX spectrum witnesses the presence of Ni, Se, C and N elements in composite materials, suggesting the successful preparation of NiSe$_2$/g-C$_3$N$_4$ composite. Furthermore, EDX elemental mapping images of as-prepared composite is measured to explore the elements distribution (Fig. 3e–h). As expected, the locations of four elements (C, N, Ni and Se) distribute uniformly in as-prepared NiSe$_2$/g-C$_3$N$_4$ nanocoral composite.

3.2. Electrochemical performances of as-prepared electrodes

As well known, an excellent OER catalyst usually exhibits low onset potential, low overpotential and high current density. Polarization curves of as-prepared catalysts are carried out in 1.0M KOH solution at scan rate of 1 mV s^{-1} (Fig. 4a). The oxidation peak before the onset potential of OER for NiSe$_2$ nanoparticles and NiSe$_2$/g-C$_3$N$_4$ nanocoral composite is attributed to the oxidation of Ni species [38,39]. It is observed that, based on the support of multi-layered g-C$_3$N$_4$, NiSe$_2$/g-C$_3$N$_4$ nanocoral composite exhibits low onset potential of 1.38 V. Furthermore, NiSe$_2$/g-C$_3$N$_4$ nanocoral composite shows lower potential (1.52 V) than those of NiSe$_2$ nanoparticles (1.63 V) and multi-layered g-C$_3$N$_4$ (1.77 V) at 40 mA cm^{-2}, and the corresponding overpotential values are calculated as 290, 400 and 540 mV, respectively, suggesting favorable OER performance of NiSe$_2$/g-C$_3$N$_4$ nanocoral composite [40]. In addition, NiSe$_2$/g-C$_3$N$_4$ nanocoral composite shows higher current density (199 mA cm^{-2}) than bare NiSe$_2$ nanoparticles (142 mA cm^{-2}) at 2.0 V, suggesting that the combination of NiSe$_2$ and g-C$_3$N$_4$ largely
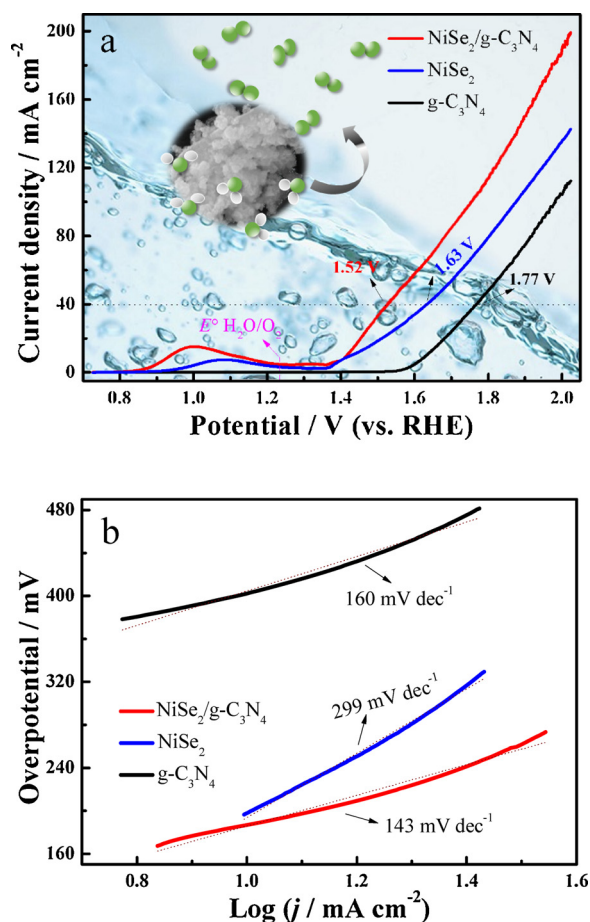
Fig. 4. Polarization curves (a) and Tafel plots (b) of as-prepared multi-layered g-C_3N_4, $NiSe_2$ nanoparticles and $NiSe_2$/g-C_3N_4 nanocoral composite.

Table 1
Electrocatalytic performances comparison of different selenide-based catalysts for OER.

Catalysts	Electrolyte	j / mA cm^{-2}	η / mV	b / mV dec^{-1}	References
$CoSe_2$/NG	0.10 M KOH	10	366	40	[10]
$CoSe_2$ nanobelts	0.10 M KOH	10	484	66	[10]
NiSe/NF	1.0 M KOH	20	270	64	[13]
$NiSe_2$/NF (Ox)	1.0 M KOH	100	390	96	[25]
$NiSe_2$/CFP	1.0 M KOH	10	220	57	[34]
$Ni_{0.5}Fe_{0.5}Se_2$	1.0 M KOH	10	235	35	[26]
NG/$NiSe_2$/NF	0.10 M KOH	20	307	89	[28]
$NiSe_2$/g-C_3N_4/NF	1.0 M KOH	40	290	143	This work

Fig. 5. Nyquist plots for as-prepared multi-layered g-C_3N_4, $NiSe_2$ nanoparticles and $NiSe_2$/g-C_3N_4 nanocoral composite. The internal illustration is magnified Nyquist plots of $NiSe_2$ nanoparticles and $NiSe_2$/g-C_3N_4 nanocoral composite.

enhances the electrocatalytic activity of composite catalyst. The more negative onset potential, lower overpotential and higher current density manifest the more highly efficient electrochemical performances of $NiSe_2$/g-C_3N_4 nanocoral composite for OER [41].

To investigate the kinetics process, Tafel plots of as-prepared catalysts are derived from polarization curves by fitting the linear regions to the Tafel equation ($\eta = \alpha + b \log j$, where η is overpotential, b the Tafel slope, j the current density, and α the Tafel constant). It is worth mentioning that OER is a complex proton-coupled multi-step reaction, therefore, ascribing one Tafel value to one specific kinetic process is impertinent. To some extent, lower Tafel value suggests lower overpotential required for catalyst to achieve higher current density at following OER process. As shown in Fig. 4b, Tafel slopes for multi-layered g-C_3N_4, $NiSe_2$ nanoparticles and $NiSe_2$/g-C_3N_4 nanocoral composite catalysts are fitted as 160, 299 and 143 mV dec^{-1}, respectively. Compared with $NiSe_2$ nanoparticles, $NiSe_2$/g-C_3N_4 nanocoral composite exhibits much lower Tafel value, suggesting faster charge transfer and attributing to the significant addition of multi-layered g-C_3N_4.

Listed in Table 1 are comparisons of OER performances of selenide-based catalysts reported in literatures. It is observed that overpotentials of as-prepared materials in this work are lower or comparable with those reported literatures, indicating that as-prepared $NiSe_2$/g-C_3N_4 nanocoral composite exhibits excellent electrochemical performance.

To obtain more kinetic information between electrolyte and electrode interface, EIS measurement is performed in the frequency range of 10^6–10^{-1} Hz at open-circuit potential with an AC-perturbation of 5 mV. The open-circuit potential values for g-C_3N_4, $NiSe_2$ and $NiSe_2$/g-C_3N_4 based electrodes are -0.129, -0.254 and -0.179 V, respectively.

Shown in Fig. 5 are corresponding fitted Nyquist plots for multi-layered g-C_3N_4, $NiSe_2$ nanoparticles and $NiSe_2$/g-C_3N_4 nanocoral composite. All Nyquist plots consist of a semicircle component at high frequency region and a straight line at low frequency region. The semicircle in the higher frequency range corresponds to the charge transfer resistance (R_{ct}) at the electrode/electrolyte interface. R_{ct} values of multi-layered g-C_3N_4, $NiSe_2$ nanoparticles and $NiSe_2$/g-C_3N_4 nanocoral composite are 157.0, 7.0 and 3.0 Ω, respectively, indicating the favorable conductivity and fast charge transfer of $NiSe_2$/g-C_3N_4 nanocoral composite.

Stability is a significant parameter to weigh effectiveness for catalyst. In this work, chronoamperometry of as-prepared $NiSe_2$/g-C_3N_4 composite is carried out at constant potential of 1.42 V (vs. RHE) to achieve current density of 10 mA cm^{-2}. As shown in Fig. 6, the current density is stable and remains 77.28% after 10 h, suggesting excellent long-term stability. The outstanding stability may owe to several reasons as follows: 1) the addition of multi-layered g-C_3N_4 with rough surface, which theoretically increases the surface activity, and thus decreases activation energy of electrode reaction; 2) the intrinsic electroactivity and satisfied conductivity of $NiSe_2$; 3) synergistic effect between $NiSe_2$ and g-C_3N_4. The stability result indicates that $NiSe_2$/g-C_3N_4 nanocoral composite is a promising OER catalyst to alleviate the dependence on noble-metal based catalysts.

4. Conclusions

In summary, a novel $NiSe_2$/g-C_3N_4 nanocoral catalyst has been fabricated via facile hydrothermal method. As-prepared $NiSe_2$/g-C_3N_4 nanocoral electrocatalyst presents highly efficient OER performances as expected. $NiSe_2$/g-C_3N_4 nanocoral shows low onset potential of 1.38 V (vs. RHE), low overpotential of 290 mV at the current density of 40 mA

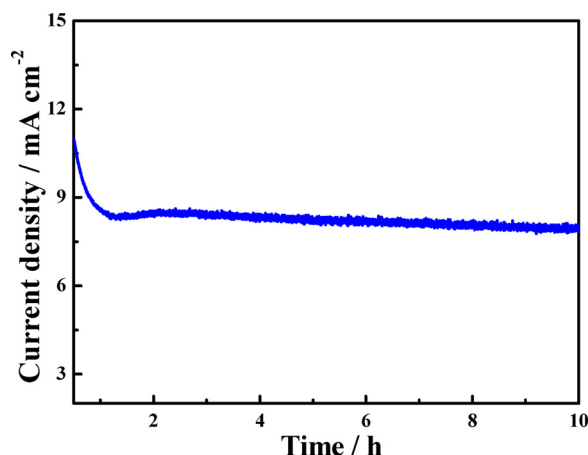**Fig. 6.** Stability study of NiSe$_2$/g-C$_3$N$_4$ nanocoral composite catalyst at constant potential of 1.42 V (vs. RHE) in 1.0 M KOH solution.

cm^{-2} and high current density of 199 mA cm^{-2} at 2.0 V (vs. RHE). In addition, NiSe$_2$/g-C$_3$N$_4$ nanocoral composite possesses excellent long-term stability in alkaline solution. All the favorable OER performances of composite catalyst are related to the support of multi-layered g-C$_3$N$_4$ and intrinsic electrocatalytic activity of NiSe$_2$ nanoparticles. The results suggest that NiSe$_2$/g-C$_3$N$_4$ nanocoral electrocatalyst is promised to be a convincing catalyst for electrocatalytic OER.

References

[1] S. Anantharaj, S.R. Ede, K. Sakthikumar, K. Karthick, S. Mishra, S. Kundu, Recent trends and perspectives in electrochemical water splitting with an emphasis on sulfide, selenide, and phosphide catalysts of Fe, Co, and Ni: a review, ACS Catal. 6 (2016) 8069–8097.

[2] J.S. Kim, B. Kim, H. Kim, K. Kang, Recent progress on multimetal oxide catalysts for the oxygen evolution reaction, Adv. Energy Mater. 8 (2018) 1702774, , https://doi.org/10.1002/aenm.201702774.

[3] G.R. Xu, J. Rai, L. Yao, Q. Xue, J.X. Jiang, J.H. Zeng, Y. Chen, J.M. Lee, Polyallylamine functionalized platinum tripods: enhancement of hydrogen evolution reaction by proton carriers, ACS Catal. 7 (2017) 452–458.

[4] R.G. Cao, J.S. Lee, M.L. Liu, J. Cho, Recent progress in non-precious catalysts for metal-air batteries, Adv. Energy Mater. 2 (2012) 816–829.

[5] L.F. Wu, X.S. Wang, Y.P. Sun, Y. Liu, J.H. Li, Flawed MoO$_2$ belts on graphene template transformated from MoO$_3$ towards hydrogen evolution reaction, Nanoscale 7 (2015) 7040–7044.

[6] X.Q. Ji, X. Ren, S. Hao, F.Y. Xie, F.L. Qu, G. Du, A.M. Asiri, X.P. Sun, Greatly enhancing the alkaline oxygen evolution reaction activity of NiCo$_2$O$_4$ by amorphous borate shell, Inorg. Chem. Front. 4 (2017) 1546–1550.

[7] S.P. Li, G. Zhang, X.M. Tu, J.H. Li, Polycrystalline CoP/CoP$_2$ structures for efficient full water splitting, ChemElectroChem 5 (2018) 701–707.

[8] J.X. Zhao, X.H. Li, G.W. Cui, X.P. Sun, Highly-active oxygen evolution electrocatalyzed by a Fe-doped NiCr$_2$O$_4$ nanoparticles film, Chem. Commun. 54 (2018) 5462–5465.

[9] A.A. Ahmed, B. Hou, H.S. Chavan, Y. Jo, S. Cho, J. Kim, S.M. Pawar, S. Cha, A.I. Inamdar, H. Kim, H. Im, Self-assembled nanostructured CuCo$_2$O$_4$ for electrochemical energy storage and the oxygen evolution reaction via morphology engineering, Small 14 (2018) 1800742, , https://doi.org/10.1002/smll.201800742.

[10] M.R. Gao, X. Cao, Q. Gao, Y.F. Xu, Y.R. Zheng, J. Jiang, S.H. Yu, Nitrogen-doped graphene supported CoSe$_2$ nanobelt composite catalyst for efficient water oxidation, ACS Nano 8 (2014) 3970–3978.

[11] X.L. Xiong, Y.Y. Ji, M.W. Xie, C. You, L. Yang, Z.A. Liu, A.M. Asiri, X.P. Sun, MnO$_2$-CoP$_3$ nanowires array: an efficient electrocatalyst for alkaline oxygen evolution reaction with enhanced activity, Electrochem. Commun. 86 (2018) 161–165.

[12] L.H. Zhuang, L. Ge, Y.S. Yang, M.R. Li, Y. Jia, X.D. Yao, Z.H. Zhu, Ultrathin iron-cobalt oxide nanosheets with abundant oxygen vacancies for the oxygen evolution reaction, Adv. Mater. 29 (2017) 1606793, , https://doi.org/10.1002/adma.

201606793.

[13] C. Tang, N.Y. Cheng, Z.H. Pu, W. Xing, X.P. Sun, NiSe nanowire film supported on nickel foam: an efficient and stable 3D bifunctional electrode for full water splitting, Angew. Chem. Int. Edit. 54 (2015) 9351–9355.

[14] M. Tahir, L. Pan, F. Idrees, X.W. Zhang, L. Wang, J.J. Zou, Z.L. Wang, Electrocatalytic oxygen evolution reaction for energy conversion and storage: a comprehensive review, Nano Energy 37 (2017) 136–157.

[15] D.F. Yan, Y.X. Li, J. Huo, R. Chen, L.M. Dai, S.Y. Wang, Defect chemistry of non-precious-metal electrocatalysts for oxygen reactions, Adv. Mater. 29 (2017) 1606459, , https://doi.org/10.1002/adma.201606459.

[16] F. Song, L.C. Bai, A. Moysiadou, S. Lee, C. Hu, L. Liardet, X.L. Hu, Transition metal oxides as electrocatalysts for the oxygen evolution reaction in alkaline solutions: an application-inspired renaissance, J. Am. Chem. Soc. 140 (2018) 7748–7759.

[17] M.Q. Yao, N. Wang, W.C. Hu, S. Komarneni, Novel hydrothermal electrodeposition to fabricate mesoporous film of Ni$_{0.8}$Fe$_{0.2}$ nanosheets for high performance oxygen evolution reaction, Appl. Catal. B Environ. 233 (2018) 226–233.

[18] Y.S. Du, G.Z. Cheng, W. Luo, Colloidal synthesis of urchin-like Fe doped NiSe$_2$ for efficient oxygen evolution, Nanoscale 9 (2017) 6821–6825.

[19] Y.Q. Zhang, M. Li, B. Hua, Y. Wang, Y.F. Sun, J.L. Luo, A strongly cooperative spinel nanohybrid as an efficient bifunctional oxygen electrocatalyst for oxygen reduction reaction and oxygen evolution reaction, Appl. Catal. B Environ. 236 (2018) 413–419.

[20] S. Yoon, J.Y. Yun, J.H. Lim, B.Y. Yoo, Enhanced electrocatalytic properties of electrodeposited amorphous cobalt-nickel hydroxide nanosheets on nickel foam by the formation of nickel nanocones for the oxygen evolution reaction, J. Alloys Compd. 693 (2017) 964–969.

[21] H. Wang, H.B. Feng, J.H. Li, Graphene and graphene-like layered transition metal dichalcogenides in energy conversion and storage, Small 10 (2014) 2165–2181.

[22] X. Zhao, X.Q. Li, Y. Yan, Y.L. Xing, S.C. Lu, L.Y. Zhao, S.M. Zhou, Z.M. Peng, J. Zeng, Electrical and structural engineering of cobalt selenide nanosheets by Mn modulation for efficient oxygen evolution, Appl. Catal. B Environ. 236 (2018) 569–575.

[23] L. Yang, Y.D. Yao, G.L. Zhu, M. Ma, W.Y. Wang, L.C. Wang, H. Zhang, Y. Zhang, Z.F. Jiao, Co doping of worm-like Cu$_2$S: an efficient and durable heterogeneous electrocatalyst for alkaline water oxidation, J. Alloys Compd. 762 (2018) 637–642.

[24] S.S. Ding, P. He, W.R. Feng, L. Li, G.L. Zhang, J.C. Chen, F.Q. Dong, H.C. He, Novel molybdenum disulfide nanosheets-decorated polyaniline: preparation, characterization and enhanced electrocatalytic activity for hydrogen evolution reaction, J. Phys. Chem. Solids 91 (2016) 41–47.

[25] X. Li, G.Q. Han, Y.R. Liu, B. Dong, X. Shang, W.H. Hu, Y.M. Chai, Y.Q. Liu, C.G. Liu, In situ grown pyramid structures of nickel diselenides dependent on oxidized nickel foam as efficient electrocatalyst for oxygen evolution reaction, Electrochim. Acta 205 (2016) 77–84.

[26] Y.S. Du, G.Z. Cheng, W. Luo, NiSe$_2$/FeSe$_2$ nanodendrites: a highly efficient electrocatalyst for oxygen evolution reaction, Catal. Sci. Technol. 7 (2017) 4604–4608.

[27] X.J. Zhang, L. Tao, P. He, X.Q. Zhang, M.Q. He, F.Q. Dong, S.Y. He, C.X. Li, H.H. Liu, S. Wang, Y. Zhang, A novel cobalt hexacyanoferrate/multi-walled carbon nanotubes nanocomposite: spontaneous assembly synthesis and application as electrode materials with significantly improved capacitance for supercapacitors, Electrochim. Acta 259 (2018) 793–802.

[28] J. Yu, Q.Q. Li, C.Y. Xu, N. Chen, Y. Li, H.G. Liu, L. Zhen, V.P. Dravid, J.S. Wu, NiSe$_2$ pyramids deposited on N-doped graphene encapsulated Ni foam for high-performance water oxidation, J. Mater. Chem. A 5 (2017) 3981–3986.

[29] P. Kumar, R. Boukherroub, K. Shankar, Sunlight-driven water-splitting using two-dimensional carbon based semiconductors, J. Mater. Chem. A 6 (2018) 12876–12931.

[30] L. Jing, W.J. Ong, R. Zhang, E. Pickwell-Macpherson, J.C. Yu, Graphitic carbon nitride nanosheet wrapped mesoporous titanium dioxide for enhanced photoelectrocatalytic water splitting, Catal. Today 315 (2018) 103–109.

[31] T. Jayaraman, A.P. Murthy, V. Elakkiya, S. Chandrasekaran, P. Nithyadharseni, Z. Khan, R.A. Senthil, R. Shanker, M. Raghavender, P. Kuppusami, M. Jagannathan, M. Ashokkumar, Recent development on carbon based heterostructures for their applications in energy and environment: a review, J. Ind. Eng. Chem. 64 (2018) 16–59.

[32] Y. Zheng, Y. Jiao, Y.H. Zhu, Q.R. Cai, A. Vasileff, L.H. Li, Y. Han, Y. Chen, S.Z. Qiao, Molecule-level g-C$_3$N$_4$ coordinated transition metals as a new class of electrocatalysts for oxygen electrode reactions, J. Am. Chem. Soc. 139 (2017) 3336–3339.

[33] J. Feng, J.B. Chen, J.L. Mu, L.D. Chen, H. Miao, E.Z. Liu, J. Fan, X.Y. Hu, A facile in situ solvothermal method for two-dimensional layered g-C$_3$N$_4$/SnS$_2$ p-n heterojunction composites with efficient visible-light photocatalytic activity, J. Nanopart. Res. 20 (2018) 38, https://doi.org/10.1007/s11051-018-4143-4.

[34] A.T. Swesi, J. Masud, W.P.R. Liyanage, S. Umapathi, E. Bohannan, J. Medvedeva, M. Nath, Textured NiSe$_2$ film: bifunctional electrocatalyst for full water splitting at remarkably low overpotential with high energy efficiency, Sci. Rep. 7 (2017) 2401, https://doi.org/10.1038/s41598-017-02285-z.

[35] Y.J. Zhong, Z.Q. Wang, J.Y. Feng, S.C. Yan, H.T. Zhang, Z.S. Li, Z.G. Zou, Improvement in photocatalytic H$_2$ evolution over g-C$_3$N$_4$ prepared from protonated melamine, Appl. Surf. Sci. 295 (2014) 253–259.

[36] W.X. Zou, B. Deng, X.X. Hu, Y.P. Zhou, Y. Pu, S.H. Yu, K.L. Ma, J.F. Sun, H.Q. Wan, L. Dong, Crystal-plane-dependent metal oxide-support interaction in CeO$_2$/g-C$_3$N$_4$ for photocatalytic hydrogen evolution, Appl. Catal. B Environ. 238 (2018) 111–118.

[37] L.X. Wang, Y. Li, X.C. Yin, Y.Z. Wang, A.L. Song, Z.P. Ma, X.J. Qin, G.J. Shao, Coral-like structured Ni/C$_3$N$_4$ composite coating: an original catalyst for hydrogen evolution reaction in alkaline solution, ACS Sustain. Chem. Eng. 5 (2017) 7993–8003.

[38] J.H. Kim, D.H. Youn, K. Kawashima, J. Lin, H. Lim, C.B. Mullins, An active nanoporous Ni(Fe) OER electrocatalyst via selective dissolution of Cd in alkaline media, Appl. Catal. B Environ. 225 (2018) 1–7.

[39] S.L. Zhao, Y. Wang, J.C. Dong, C.T. He, H.J. Yin, P.F. An, K. Zhao, X.F. Zhang, C. Gao, L.J. Zhang, J.W. Lv, J.X. Wang, J.Q. Zhang, A.M. Khattak, N.A. Khan, Z.X. Wei, J. Zhang, S.Q. Liu, H.J. Zhao, Z.Y. Tang, Ultrathin metal-organic framework nanosheets for electrocatalytic oxygen evolution, Nat. Energy 1 (2016) 1–10.

[40] J. Wang, F. Xu, H.Y. Jin, Y.Q. Chen, Y. Wang, Non-noble metal-based carbon composites in hydrogen evolution reaction: fundamentals to applications, Adv. Mater. 29 (2017) 1605838, , https://doi.org/10.1002/adma.201605838.

[41] N.T. Suen, S.F. Hung, Q. Quan, N. Zhang, Y.J. Xu, H.M. Chen, Electrocatalysis for the oxygen evolution reaction: recent development and future perspectives, Chem. Soc. Rev. 46 (2017) 337–365.